JOURNAL OF GUIDANCE, CONTROL, AND DYNAMICS
Vol. 16, No. 3, May-June 1993

Stable Orbits About the Martian Moons

William E. Wiesel*
Air Force Institute of Technology, Wright-Patterson Air Force Base, Ohio 45433

A dynamics model of a satellite of Phobos or Deimos is developed that includes Mars' gravity and oblateness and the moon's orbital eccentricity and its nonspherical shape. Two special cases of the dynamics are studied. If the moon's eccentricity is zero, then we have an autonomous system and families of periodic orbits exist. If the eccentricity is not zero, we have a time-periodic dynamical system which still permits isolated periodic orbits. The zero eccentricity periodic orbits are constructed and found to be stable at any period. In addition, the most important nonzero eccentricity period orbits are given. Sensitivity to poorly known system parameters is explored, and accuracy requirements for spacecraft insertion maneuvers are established. Stable orbits exist about both moons and are well enough known to be used by unmanned spacecraft.

Introduction

THE small moons of Mars, Phobos and Deimos, are of interest for several reasons. From a scientific perspective, they are believed to be captured asteroids and can be studied as a byproduct of any Mars mission. From an engineering point of view, they are potentially valuable for resources to supply manned missions to Mars. The total Δv required to reach these objects from Earth orbit is less than that required to reach the lunar surface, although the trip times are longer.

They are also interesting from an orbital mechanics perspective. Dobrovolskis and Burns[1] have pointed out that Phobos virtually fills its own Roche lobe, whereas Deimos is only a factor of two smaller than its Roche lobe. In other terms, the classical L_1 and L_2 libration points are located about 3 km above Phobos' surface and can be reached with a 5 ms^{-1} velocity change. The weak gravity field of these objects makes a slow drifting flyby possible but would seem to rule out orbiting these bodies. However, this is not the case.

Earlier work on orbiting the Martian moons has been reported by Jannson and Wiesel,[2] using the restricted three-body problem with the moon's oblateness included. By means of the surface of section technique, a survey of possible motions was carried out for both Phobos and Deimos. For Phobos the only stable regions existed about retrograde periodic orbits. Results for Deimos were similar, but in addition a small stable area of retrograde Keplerian motion existed within a few kilometers of that moon. The stable retrograde periodic orbit families have been calculated by Luria,[3] using the restricted problem with the moon's oblateness included in the model.

In this paper we will considerably expand the scope of the dynamics model and explore stability regions and navigational requirements for placing a spacecraft in orbit about these objects.

Dynamics

Our fundamental aim shall be to include as much of the significant dynamics as possible in our model, so long as periodic orbits can still be found. In this section we derive the Hamiltonian for the spacecraft motion. We will assume that the orbit of the moon lies in the equator plane of Mars, and that it is an elliptical orbit with semimajor axis a and eccentricity e, precessing under the influence of Mars dynamical oblateness J_2. Write the longitude of perimartem as $\tilde{\omega}$, $\mathfrak{M}$ for the mass of Mars, $\mathfrak{R}$ for Mars' equatorial radius, and G for the gravitational constant. Let the mass of the moon be m, and in analogy with the restricted three-body problem, define $\mu = m/(\mathfrak{M} + m)$. Then the moon's mean anomaly rate is

$$\dot{M} = \sqrt{G(\mathfrak{M} + m)}\left\{a^{-3/2} + \frac{3J_2\mathfrak{R}^2}{2a^{7/2}(1-e^2)^{3/2}}\right\} \tag{1}$$

the well-known Kozai mean motion, whereas the orbital apse rate is given by

$$\dot{\tilde{\omega}} = \sqrt{G(\mathfrak{M} + m)}\,\frac{3J_2\mathfrak{R}^2}{2a^{7/2}(1-e^2)^2} \tag{2}$$

As shown in Fig. 1, place a rotating reference frame $\boldsymbol{a}$ on the moon, aligned with the principal axis frame of that body, and rotating with angular rate Ω. This will be the frame used to define the spacecraft radius vector

$$\boldsymbol{R} = x\boldsymbol{a}_1 + y\boldsymbol{a}_2 + z\boldsymbol{a}_3 \tag{3}$$

where x, y, and z are the generalized coordinates for the spacecraft relative to the moon. The $\boldsymbol{a}_1$ axis aligns with $\boldsymbol{D}$, the Mars-moon radius vector, at perimartem and apomartem, in the standard gravity-gradient stable orientation, whereas $\boldsymbol{a}_3$ is the orbit normal vector. To align the principal axis frame with the radius at each perimartem, we must have $\nu + \tilde{\omega} - \Omega t = 0$ at the end of each anomalistic orbital period $\tau = 2\pi/\dot{M}$, where ν is the orbital true anomaly. This immediately gives the moon's (constant) rotation rate as

$$\Omega = \dot{M} + \dot{\tilde{\omega}} \tag{4}$$

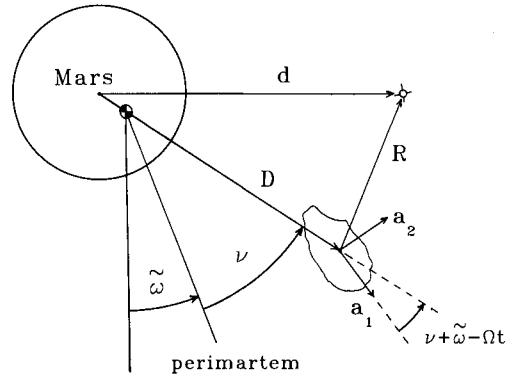

Fig. 1 Geometry for a Martian moon rotating at uniform rate Ω in an eccentric orbit.

Received April 17, 1991; revision received April 12, 1992; accepted for publication June 26, 1992.

*Professor of Astronautical Engineering, Department of Aeronautical and Astronautical Engineering. Member AIAA.

The inertial angular velocity of the $\boldsymbol{a}$ frame is then

$$\omega^{ai} = \Omega \boldsymbol{a}_3 \tag{5}$$

which is needed for the calculation of the spacecraft's inertial velocity.

Since the spacecraft's position is referenced to the rotating $\boldsymbol{a}$ frame centered on the moon, considerable care must be exercised in calculating its inertial velocity. The inertial origin for this problem is located at the Mars-moon center of mass, shown in Fig. 1. The position vector of the moon relative to Mars' center, expressed in the $\boldsymbol{a}$ frame, is given by

$$\boldsymbol{D} = D\cos(\nu + \tilde{\omega} - \Omega t)\boldsymbol{a}_1 + D\sin(\nu + \tilde{\omega} - \Omega t)\boldsymbol{a}_2 \tag{6}$$

where D is the moon's orbital radius. But the inertial position vector of the satellite is $\boldsymbol{r} = (1-\mu)\boldsymbol{D} + \boldsymbol{R}$, so its inertial velocity is given by

$$\begin{aligned}\mathbf{v} &= \frac{{}^{i}\mathrm{d}}{\mathrm{d}t}[(1-\mu)\boldsymbol{D} + \boldsymbol{R}] = \frac{{}^{a}\mathrm{d}}{\mathrm{d}t}[(1-\mu)\boldsymbol{D} + \boldsymbol{R}] + \omega^{ai} \\ &\times [(1-\mu)\boldsymbol{D} + \boldsymbol{R}] = [\dot{x} - \Omega y + (1-\mu)\dot{D}\cos(\nu + \tilde{\omega} - \Omega t) \\ &- (1-\mu)D(\dot{\nu} + \dot{\tilde{\omega}})\sin(\nu + \tilde{\omega} - \Omega t)]\boldsymbol{a}_1 + [\dot{y} + \Omega x \\ &+ (1-\mu)\dot{D}\sin(\nu + \tilde{\omega} - \Omega t) \\ &+ (1-\mu)D(\dot{\nu} + \dot{\tilde{\omega}})\cos(\nu + \tilde{\omega} - \Omega t)]\boldsymbol{a}_2 + \dot{z}\boldsymbol{a}_3\end{aligned} \tag{7}$$

Although the moon's orbit is planar and all spacecraft orbits constructed in this paper will be planar, including the z component in the dynamics will allow us to study out-of-plane stability. The moon's orbital radius D, radial velocity $\dot{D}$, true anomaly ν, and orbital angular rate $\dot{\nu}$ are all obtained from the usual two-body formulas

$$D = \frac{a(1-e^2)}{1 + e\cos\nu} \tag{8}$$

$$\dot{D} = \left\{\frac{G(\mathfrak{M} + m)}{a(1-e^2)}\right\}^{1/2} e\sin\nu \tag{9}$$

$$\dot{\nu} = \frac{1}{D}\left\{\frac{G(\mathfrak{M} + m)}{a(1-e^2)}\right\}^{1/2}(1 + e\cos\nu) \tag{10}$$

Of course, ν is obtained from the time by solving Kepler's equation in the usual fashion, using the mean anomaly rate (1). All of these quantities are periodic functions of time, with period equal to the anomalistic period of the moon.

With the inertial velocity in hand, the kinetic energy per unit mass of spacecraft is just $T = \mathbf{v}\cdot\mathbf{v}/2$. This enables us to calculate the canonical momenta for this problem using $p_i = \partial T/\partial\dot{q}_i$, where the spacecraft coordinates are x, y, and z. The canonical momenta are given by

$$\begin{aligned}p_x &= \dot{x} - \Omega y + (1-\mu)\dot{D}\cos(\nu + \tilde{\omega} - \Omega t) \\ &- (1-\mu)D(\dot{\nu} + \dot{\tilde{\omega}})\sin(\nu + \tilde{\omega} - \Omega t) \\ p_y &= \dot{y} + \Omega x + (1-\mu)\dot{D}\sin(\nu + \tilde{\omega} - \Omega t) \\ &+ (1-\mu)D(\dot{\nu} + \dot{\tilde{\omega}})\cos(\nu + \tilde{\omega} - \Omega t) \\ p_y &= \dot{z}\end{aligned} \tag{11}$$

Comparing Eq. (11) to Eq. (7) we see that these are just the components of the inertial velocity resolved along the $\boldsymbol{a}$ frame axes.

The satellite's potential energy includes the dominant ellipsoidal terms for the moon's gravity field[4] and the Newtonian and oblateness terms for Mars. Write A, B, and C for the moon's principal moments of inertia. Then the potential energy for the satellite can be written as

$$\begin{aligned}V &= -\frac{G\mathfrak{M}}{d} - \frac{G\mathfrak{M}J_2\mathfrak{R}^2}{2d^3} - \frac{Gm}{R} + \frac{G}{4R^3}(A + B + C) \\ &- \frac{3G}{4R^5}\{x^2(B + C - A) + y^2(A + C - B) \\ &+ z^2(A + B - C)\}\end{aligned} \tag{12}$$

The radius vector from the moon to the satellite is, by inspection of Fig. 1,

$$R^2 = x^2 + y^2 + z^2 \tag{13}$$

and that from the center of Mars to the satellite is

$$\begin{aligned}d^2 &= [x + D\cos(\nu + \tilde{\omega} - \Omega t)]^2 \\ &+ [y + D\sin(\nu + \tilde{\omega} - \Omega t)]^2 + z^2\end{aligned} \tag{14}$$

Now, with the kinetic and potential energies calculated, the Lagrangian function is just $\mathfrak{L} = T - V$. This is converted into a Hamiltonian function by

$$\mathfrak{H} = \sum_i p_i\dot{q}_i - \mathfrak{L} \tag{15}$$

after the generalized velocity components are eliminated in favor of the momenta. Calculation gives the final result

$$\begin{aligned}\mathfrak{H} &= \tfrac{1}{2}(p_x^2 + p_y^2 + p_z^2) \\ &+ p_x\{\Omega y - (1-\mu)\dot{D}\cos(\nu + \tilde{\omega} - \Omega t) \\ &+ (1-\mu)D(\dot{\nu} + \dot{\tilde{\omega}})\sin(\nu + \tilde{\omega} - \Omega t)\} \\ &+ p_y\{-\Omega x - (1-\mu)\dot{D}\sin(\nu + \tilde{\omega} - \Omega t) \\ &- (1-\mu)D(\dot{\nu} + \dot{\tilde{\omega}})\cos(\nu + \tilde{\omega} - \Omega t)\} \\ &- \frac{G\mathfrak{M}}{d} - \frac{G\mathfrak{M}J_2\mathfrak{R}^2}{2d^3} - \frac{Gm}{R} + \frac{G}{4R^3}(A + B + C) \\ &- \frac{3G}{4R^5}\{x^2(B + C - A) + y^2(A + C - B) \\ &+ z^2(A + B - C)\}\end{aligned} \tag{16}$$

Note that $\dot{D}$, $\dot{\nu}$, and $\dot{\tilde{\omega}}$ are known functions of time through Eqs. (9), (10), and (2), so the Hamiltonian does not have velocity components present. Equations of motion are then given by the usual Hamilton's equations

$$\dot{q}_i = \frac{\partial\mathfrak{H}}{\partial p_i}, \qquad \dot{p}_i = -\frac{\partial\mathfrak{H}}{\partial q_i} \tag{17}$$

where q_i is any one of the coordinates x, y, or z. The equations of motion can be assembled into state vector form $\dot{\boldsymbol{x}} = \boldsymbol{F}(\boldsymbol{x}, t)$. In addition, the equations of variation for the state transition matrix have been constructed, where

$$\dot{\Phi} = A(t)\Phi, \qquad \Phi(t=0) = I \tag{18}$$

where I is the identity matrix, and $A(t) = \nabla_x F$.

The preceding dynamical system possesses an integral of the motion only when the moon's orbit is circular. Since we are interested in the noncircular case, this leaves us without any useful control on the accuracy of numerical integrations. However, the Hamiltonian formulation does lend itself to careful and systematic checking of the code. The equations of motion are partial derivatives of the Hamiltonian function. If

Table 1 Martian system parameters: $G\mathfrak{M}$, 42,828.44 km^3/s^2 and $J_2\mathfrak{R}^2$, 2.25689×10^4 km^2

	Phobos	Deimos
Sidereal period, s	27,553.843	109,074.876
Anomalistic period, s	27,564.449	109,081.585
a, km	9,378.53856	23,459.00624
e	0.015	0.0005
Gm, km^3/s^2	7.206×10^{-4}	8.8×10^{-5}
X axis, km	13.4	7.5
Y axis, km	11.2	6.1
Z axis, km	9.2	5.2
GA, km/s^2	3.027×10^{-2}	1.13×10^{-3}
GB, km/s^2	3.807×10^{-2}	1.47×10^{-3}
GC, km/s^2	4.395×10^{-2}	1.64×10^{-3}

this function is also programmed, its partial derivatives can be calculated numerically and compared with the equations of motion. Changing system parameters can make normally small terms dominant, and programming errors can be quickly found. The A matrix is the partial derivatives of the equations of motion, so this method can be repeated to check the equations of variation (18). This gives a high degree of confidence that the dynamics are correctly programmed and reduces hand checking to the Hamiltonian function alone.

This dynamical system has two important special cases. If the moon is placed in a circular orbit about Mars ($e = 0$) then $\nu = M$ and $\dot{\nu} = \dot{M}$. The moon's orbital radius D is constant, and the argument $\nu + \tilde{\omega} - \Omega t = 0$ is zero for all time. In this case all time dependence vanishes from the Hamiltonian, and it is a constant of the motion. (In fact, if the moon's moments of inertia and J_2 are also set equal to zero, we have the restricted three-body problem.) This system (zero eccentricity, moments of inertia A, B, C included, but Mars' J_2 omitted) has been studied by Jannson and Wiesel[2] using the surface of section technique. If the eccentricity of the moon is not zero, then Eq. (16) is a time-periodic system, with a period equal to the anomalistic period of the moon's orbit. Both types of systems admit periodic orbits, in the former case in one parameter families, whereas in the latter case only as isolated individuals at periods resonant with the period of the moon's orbit.

System parameters adopted for this problem are compiled in Table 1. Data for Mars's gravity field are from Christensen and Balmino.[5] The sidereal period for the two moons is available from many sources, for example, the *American Ephemeris and Nautical Almanac*, and is the fundamental observed quantity. The value cited for the semimajor axis is derived from the fact that the sidereal period is $2\pi/(\dot{M} + \dot{\tilde{\omega}})$. It is needed to be the cited number of digits so that the system frequencies can be recalculated from it. The sidereal period is different from the anomalistic period $2\pi/\dot{M}$, which is the period of the Hamiltonian system (16). The anomalistic period is slightly longer, since the moon must spend extra time to catch up with the advancing perimartem. The gravitational parameters for Deimos are from the Voyager program.[6] But we have adopted the Soviet Phobos mission result for Phobos' mass,[7] since it comes from tracking data obtained in a slow approach. For comparison the Voyager result, derived from far faster flyby trajectories, is about 8% smaller. Moments of inertia have been calculated from the moon's mass and axis lengths, employing the assumption that it is a uniform density triaxial ellipsoid. Axis lengths cited in the table are from Thomas.[8] The Phobos axes differ from the work of Duxbury[9] by at most 100 m.

Periodic Orbits

Periodic orbits can be constructed by solving a boundary value problem. We can begin with initial conditions $y = 0$, $p_x = 0$, $z = 0$, $p_z = 0$, and determine x and p_y at $t = 0$ to force $p_x(\tau) = 0$, $y(\tau) = 0$, where τ is the period of the desired orbit. Because of the reflection symmetry, this is sufficient to ensure that the entire orbit closes on itself at $t = \tau$. In the time-independent case τ can be chosen at will, whereas in the time-dependent case it must be a multiple of the anomalistic period. If the state transition matrix Φ is propagated along with the trajectory, it is simple to extract the four components of Φ necessary to determine corrections to x and p_y at $t = 0$ to drive $y = 0$ and $p_x = 0$ at $t = \tau$. Once the periodic orbit iteration has converged, stability can be determined by calculating the Poincaré exponents by use of Floquet theory.[10]

Figure 2 shows the period τ in hours and the velocity with respect to Phobos

$$v_y = p_y - (1 - \mu)\Omega D \tag{19}$$

at injection on the x axis. [Of course, $(1 - \mu)\Omega D$ is just Phobos' mean orbital speed.] This family of periodic orbits is stable (including the out-of-plane z direction) and symmetric. The orbital period starts at about 8400 s for the smallest orbit outside Phobos, and asymptotically approaches Phobos' orbital period as the size of the retrograde orbit grows. Once more than a few moon radii out, these orbits are better characterized as elliptical orbits about Mars which have the same period as Phobos and which encircle the moon. This accounts for the asymptotic approach to the moon's orbital period for large radius, and emphasizes the weakness of the moon's gravitational field. The oblateness terms, however, do make a measurable difference for close orbits and must be included. The figure shows three curves for both τ and v_y at injection. These correspond to our adopted value for the mass of Phobos, the Voyager result (8% smaller), and a value 8% larger than the adopted m value. The convergence of the curves for orbital radii greater than about 50 km again emphasizes the weakness of the moon's gravity. Also plotted as dotted curves are the expected Keplerian values of τ and v_y, assuming Pho-

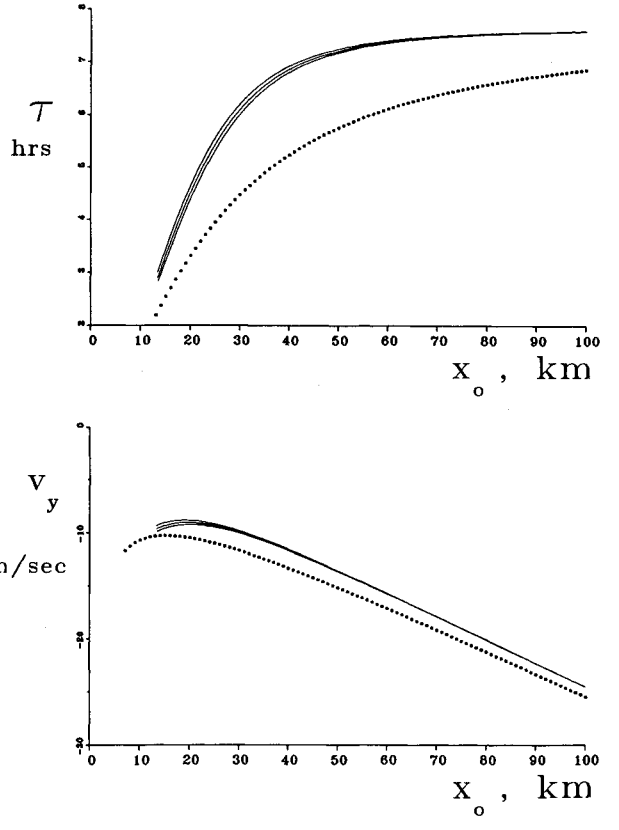

Fig. 2 Period τ and speed with respect to Phobos v_y for zero eccentricity periodic orbits about Phobos: outer two curves are ±8% variations on the nominal Phobos mass, and dotted curves show Keplerian values.

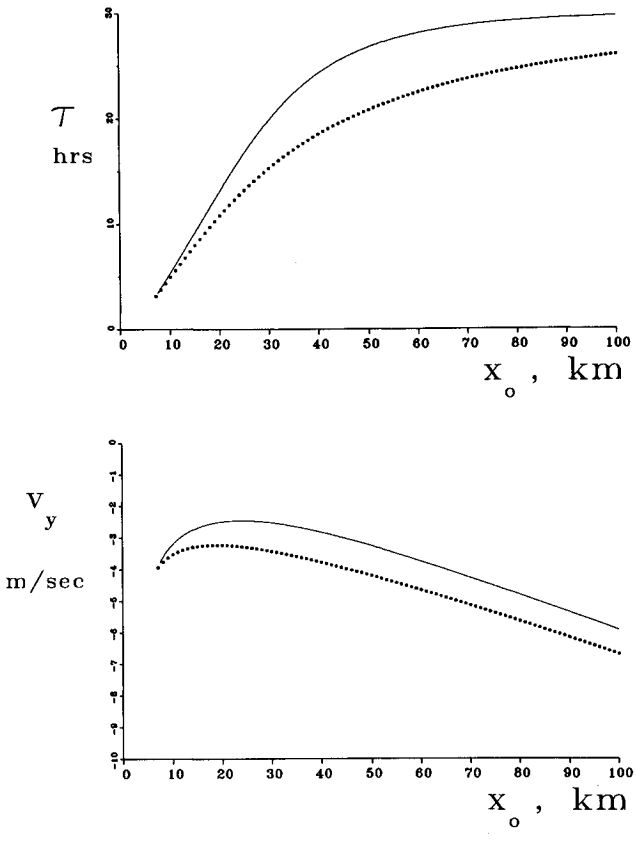

Fig. 3 Period τ and speed with respect to Deimos v_y for zero eccentricity periodic orbits: dotted curves are Keplerian predictions.

bos is a point mass and remembering that we are working in a rotating frame. The mismatch of the curves shows that a Phobos orbiter is far from being a point mass problem.

Figure 3 shows similar results for a Deimos orbiter. The closer match between the zero eccentricity periodic orbits and the Keplerian predictions shows that there is a small area of two-body-like behavior close to Deimos. Again, the period τ asymptotically approaches the period of Deimos, and in the far region the spacecraft is really a Mars orbiter that encircles Deimos. Also, as with Phobos, the stability analysis shows the orbits to be stable at all distances from Deimos (including the out-of-plane direction), except for a tiny region within a few hundred meters of the surface.

Orbits from these one parameter families that are resonant with the anomalistic orbital period of the moon [the period of the system (16)] can be expected to continue into isolated periodic orbits when the moon's eccentricity is introduced. Each resonant zero eccentricity orbit will generate two periodic orbits when the eccentricity is not zero, corresponding to starting the spacecraft on the two ends of the orbit on the x axis when the moon is at perimartem. Initial conditions for several of these orbits are shown in Table 2, along with their stability. Figure 4 shows three outer periodic orbits for Phobos, along with the moon's profile. (The other three periodic orbits are very close to the three shown, but 180 deg out of phase.) The plot has been carefully constructed to equalize the x and y axis scales, and the trajectories are not close to circular orbits about Phobos. Instead, these orbits are nearly ellipses centered on Phobos with an axis ratio of nearly 2:1. This is the behavior of a slightly elliptical orbit seen in a reference frame rotating with the mean orbital speed, as in the Clohessy-Wiltshire description of relative motion near a circular orbit. Even close to Phobos, then, Mars' gravity is dominant.

Since the zero eccentricity problem has an integral of the motion, two of its Poincaré exponents are zero, and these correspond to the freedom to start the orbit at any initial time. This freedom disappears when the eccentricity is not zero, but

Table 2 Periodic orbits

Moon	Resonance	x, km	p_y, km/s	Stable
Phobos	2:1	17.341052	2.1609408	No
Phobos	2:1	−21.939726	2.1767347	Yes
Phobos	3:2	23.049392	2.1608168	Yes
Phobos	3:2	−28.327744	2.1771422	No
Phobos	4:3	27.273497	2.1604181	Yes
Phobos	4:3	−32.771699	2.1776645	No
Deimos	2:1	22.838831	1.3493896	Yes
Deimos	2:1	−24.892825	1.3542208	No
Deimos	3:2	30.697729	1.3493143	Yes
Deimos	3:2	−32.991132	1.3543318	No
Deimos	4:3	35.896604	1.3491735	Yes
Deimos	4:3	−38.312273	1.3544874	No

the Poincaré mode should still closely correspond to an in-track displacement. All of the "unstable" orbits have just one pair of real Poincaré exponents, corresponding to the in-track mode. These are numerically quite small, and this has two implications. First, it is difficult to even claim that an instability is present, since the root may not be accurately calculated by the eigenvalue software. Second, if an instability is present, it takes a long time to grow to significant size. The other two pairs of exponents, relatively much larger, are still stable and easily recognized as the former $e = 0$ modes, so an unstable orbit at worst seems to drop out of synchronization with the moon's perimartem passage. It need not escape.

Although these orbits are exact periodic solutions to the full system (16), there are relatively few of them. They do, however, serve to point out how stable regions change when the eccentricity is introduced. It was found after much calculation that a very good prediction of these orbits can be made if 1) the x value is unchanged from the $e = 0$ case, and 2) the p_y value is corrected to include the moon's higher speed at perimartem. We will find this fact useful in the next section to study nonresonant stability regions.

Long-Term Stability

In an earlier work,[2] the surface of section technique was employed to map stable regions in the case where the moon was in a circular orbit. When the eccentricity of the moon is

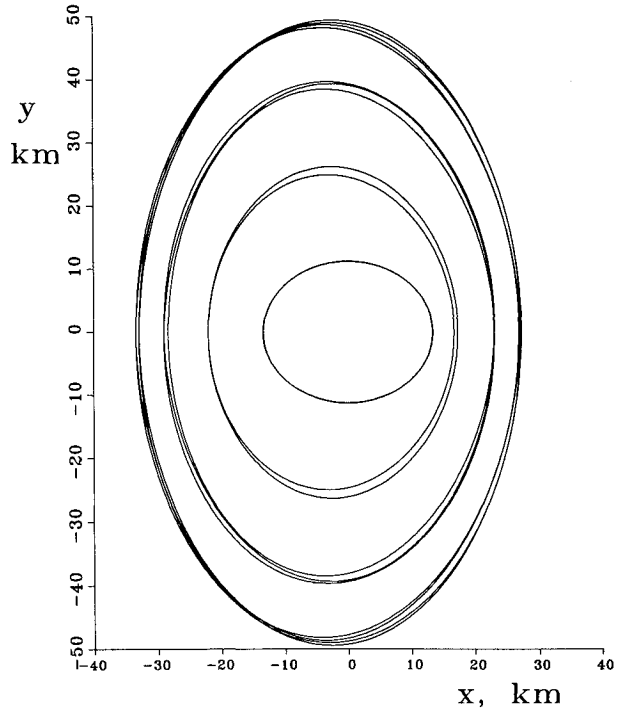

Fig. 4 Three periodic orbits about Phobos in the eccentric case; in order of radius, these are the 2:1, 3:2, and 4:3 orbits with starting position on the positive x axis.

included, the Hamiltonian becomes time dependent and is no longer a constant of the motion. With no known integrals of the motion, it is no longer possible to construct a true surface of section. So-called "first return maps" can be constructed, but they are difficult to interpret. We have adopted another tack in attempting to map stable regions.

The basic problem is that we know only six solutions to the system (16) when the eccentricity is nonzero. Ideally, we would wish to know the entire volume of initial conditions that will lead to long-term stability. Integrating trial orbits to solve this problem would entail searching a six-dimensional space of initial conditions for the three-dimensional problem, or a four-dimensional space for the planar problem. This increases by one dimension if initial conditions are chosen at different phases of the moon's orbit about Mars. To reduce the scope of this search, we have restricted ourselves to the planar problem and considered only initial conditions at perimartem. Furthermore, we have only searched the x and p_y initial conditions, as these are the nonzero initial conditions when periodic orbits are constructed. Imagine that these represent the injection conditions for a spacecraft approaching one of the moons and attempting to maneuver into a stable orbit just at the moment of perimartem. We will assume that the other initial conditions $y = 0$ and $p_x = 0$ are perfectly met, although the method described subsequently can also be used to search these axes as well.

There still remains the question of the existence of stable orbits away from the periodic solutions to the full problem. The zero eccentricity families of periodic orbits have been used as a set of trial initial conditions to search for stable solutions to the full nonzero eccentricity problem. It was quickly found, however, that the zero eccentricity initial conditions are not good predictors of stable behavior when the eccentricity is not zero. In fact, it is difficult with the zero eccentricity initial conditions to find any stable orbits unless p_y is varied. Varying p_y stable regions were found which showed systematic offsets in velocity by about $+32.2$ ms^{-1} for Phobos and $+0.677$ ms^{-1} for Deimos. These numbers are just the extra speed possessed by each moon at perigee over the circular orbital speed. So the p_y initial conditions from the zero eccentricity families were modified by adding the extra perimartem velocity, and large stable regions then became apparent. This mirrors the earlier result with the nonzero eccentricity periodic orbits, where keeping the same x initial condition but adding the perimartem velocity increment was found to be a good predictor of the actual periodic orbit initial conditions.

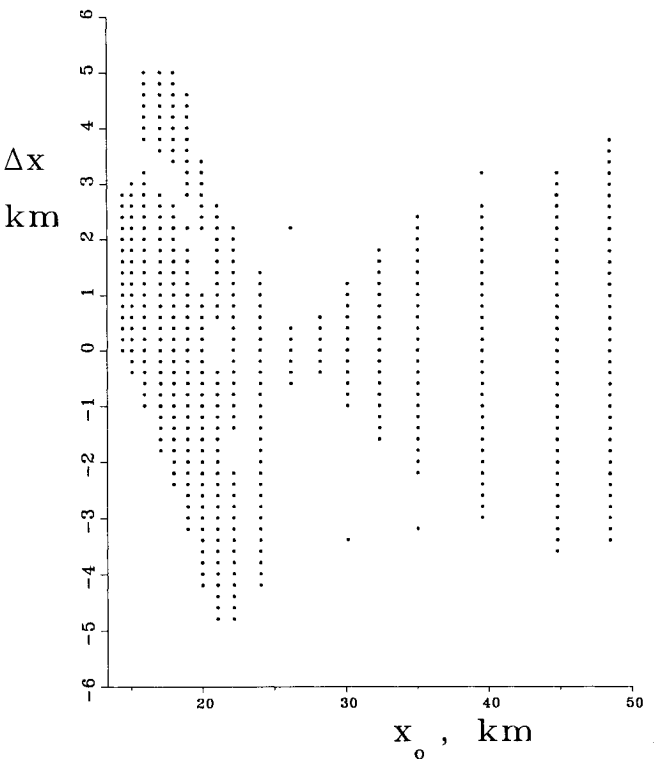

Fig. 5 Injection radius error Δx vs injection radius x_0: plotted points are trajectories which remain in Phobos' vicinity for 25 days without collision.

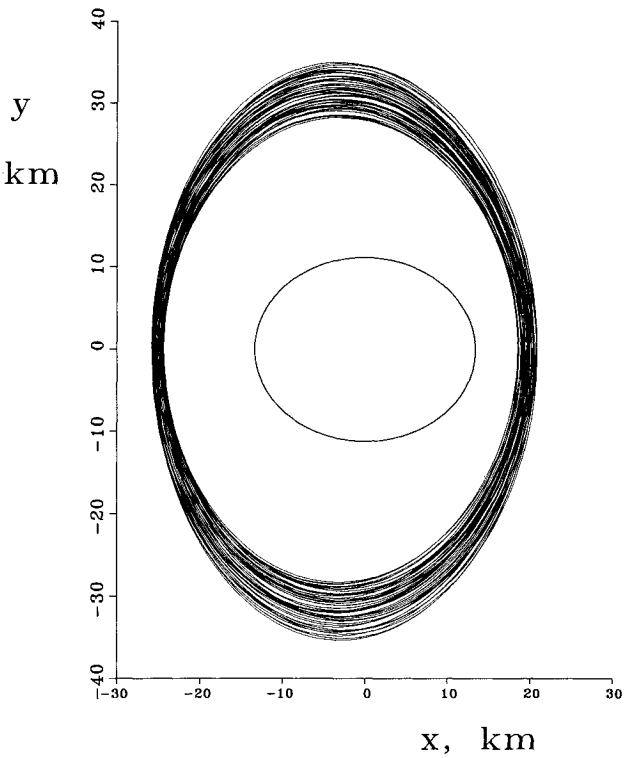

Fig. 6 Ten days of orbital behavior for a stable trajectory near the 2:1 resonant orbit.

We have made two series of numerical integrations with these initial conditions. In the first set, the modified p_y value is held constant, and the value of x_0 at injection was varied. These integrations were for progressively longer times, culminating in 25-day numerical integrations of the orbits. Figure 5 shows the final result for Phobos, where plotted points represent orbits which avoided collision or ejection for the full time interval. The stable region is very broad in Δx; in many places an error of several kilometers in injection distance still leads to a stable orbit. This is understandable when we realize that p_y varies by only a few meters per second over the entire range of distance plotted in this figure. Still, two distinct stability regions can be discerned, the first out to about 28-km radius from Phobos and the second beyond that. The first region contains the stable periodic orbits calculated in the last section. The second region can be thought of as the Mars dominated area, where the orbits are essentially slightly elliptical orbits about the planet that encircle the moon.

By performing successively longer integrations, the "mortality rate" could be assessed. Integrations terminating after 10 days produced plots essentially identical to the 25-day results. Several orbits that were stable for 25 days were continued to 90 days without escapes or collisions. Although this does not prove stability "forever," it does establish that some orbits persist long enough to survive through solar conjunction seen from Earth without active intervention by ground controllers. Figure 6 shows the trajectory for one long integration. It is an orbit near the 2:1 resonance, and the plot shows 10 days of orbital behavior.

Figure 7 gives the stable area near Phobos when the initial p_y velocity is varied, holding the injection radius x_0 constant. Again two stable regions can be seen, one associated with the periodic orbits and another at larger distances. Obviously,

from both Figs. 5 and 7, an injection radius of 28 km is a very poor choice. The bad news in Fig. 7 is that injection speed must be controlled to within a fraction of a meter per second to establish a stable orbit, even at larger orbital radii. This appears to be somewhat challenging, but several factors should make it practical. Approach to injection can be made quite slowly over several days, with tracking of landmarks on the surface of Phobos supplying very precise navigational data. The small maneuvers required for injection will probably be performed with the attitude control system, making delicate control possible. In the outer stable area orbital periods about Phobos are 6–8 h, making several navigational update cycles possible in the first orbit, even allowing for light travel time from Earth to Mars and back. Finally, any reasonable spacecraft can execute an emergency "high G" abort with its attitude thrusters in the weak gravity of Phobos.

Figures 8 and 9 show the analogous results for Deimos. The injection limits for changes in radius x_0 are very broad, since the momentum p_y varies even less than at Phobos. Figure 9 shows the momentum stability regions for Deimos. Injection again requires maneuver precision of 10 cm s^{-1} or better, but the same considerations for Phobos apply here as well, with the added benefits of longer orbital period, weaker moon gravity, and a location less deep into Mars' gravity well. There are now three distinct regions of stable behavior. The innermost is the region of Keplerian behavior observed by Jannson and Wiesel. From 20 to 35 km in radius there is a region containing the strongest resonant orbits, and beyond 35 km is the region totally dominated by Mars.

There are still other perturbations that have been omitted from our model. These include solar perturbations, the effects of the slight inclinations of the moons' orbit, other Mars gravity terms, periodic J_2 perturbations on the moons' orbits, and higher-order mass integrals for the moons themselves. The first four of these should be very small, since the orbits we have explored lie very close to the moon itself, and solar and Martian gravity should have virtually equal influence on both the moon and the spacecraft. Higher-order potential expansions have been given for Phobos by Duxbury,[9] although we have elected to not use them here. Their accurate determination would be a product of any Mars moon orbiter.

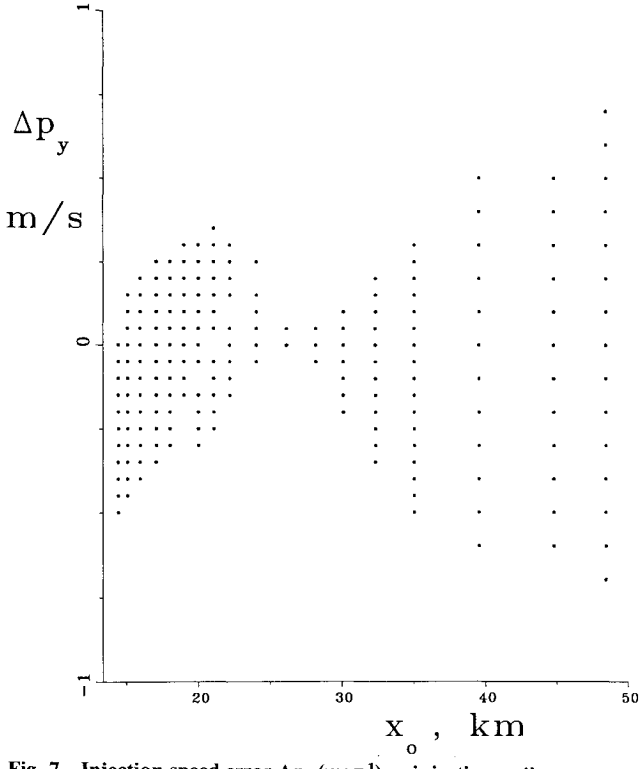

Fig. 7 Injection speed error Δp_y (ms^{-1}) vs injection radius x_0: orbits surviving for 25 days are plotted.

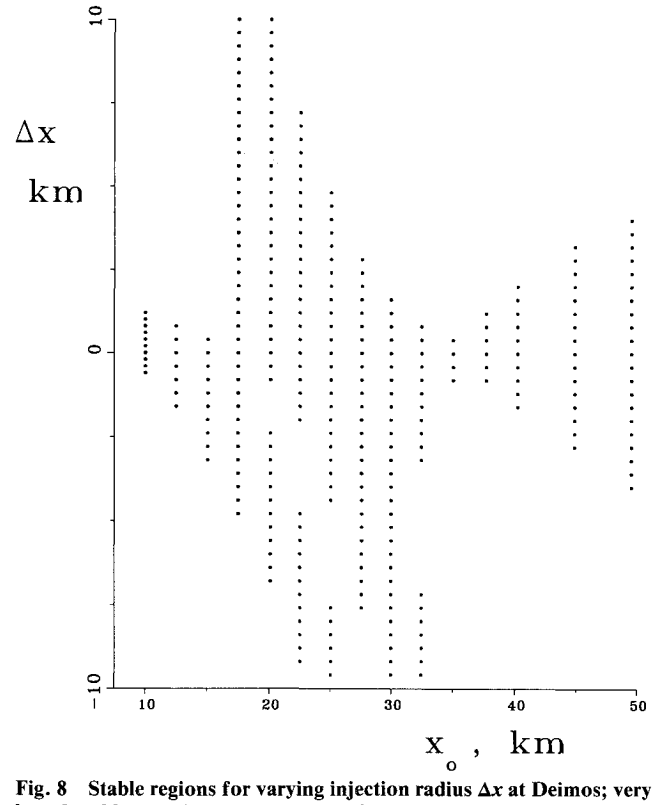

Fig. 8 Stable regions for varying injection radius Δx at Deimos; very broad stable area is a consequence of the nearly flat orbital velocity curve with respect to Deimos.

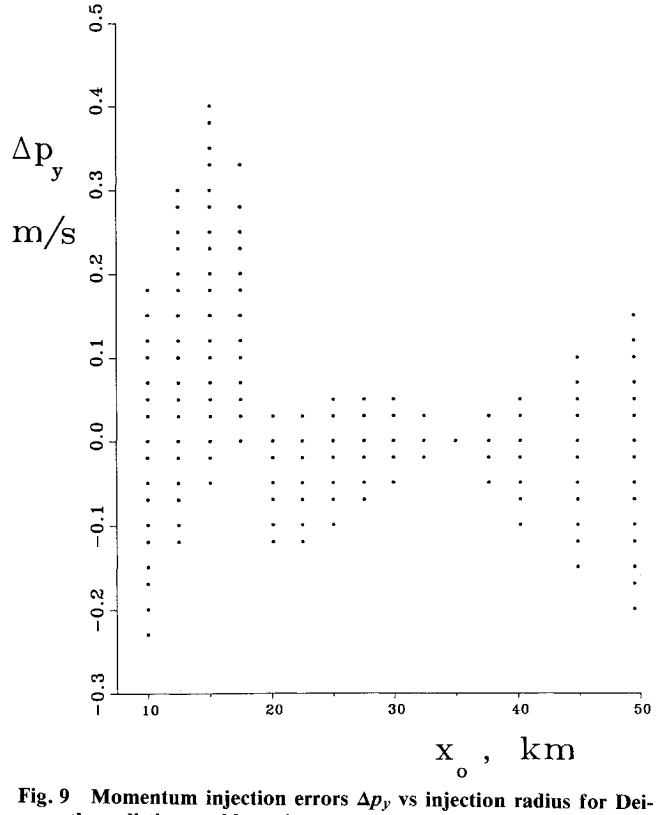

Fig. 9 Momentum injection errors Δp_y vs injection radius for Deimos: three distinct stable regions are apparent.

Phobos Orbiter

These results demonstrate that a Phobos orbiter is indeed feasible. It would supply valuable information for the scientific community on the structure and composition of what is probably a captured asteroid. Furthermore, it would explore the feasibility of using Phobos resources as an aid in Martian exploration. One of the primary missions of a Phobos orbiter

would be to determine the internal structure of the moon, and one way to do this is through determining the higher-order mass integrals through spacecraft tracking. However, the higher-order mass effects are not dominant at distances of 30–100 km, where the orbit is basically an orbit about Mars itself. A Phobos orbiter can begin its mission in a high altitude orbit and enter the closer orbits only after Phobos' gravity field is well characterized.

From a low altitude Phobos orbit, the instrument suite could include not only the usual imaging and remote sensing devices, but several penetrometers could be used to construct a global seismic net to explore the internal structure of this object. Gamma ray scattering devices on the penetrometers could characterize surface composition. Perhaps the flight portion of the mission could even terminate with a soft landing. A Phobos orbiter could be a valuable precursor mission for manned exploration of the red planet, as well as being a productive and exciting scientific mission.

Conclusions

We have developed two self-consistent dynamical models for a satellite of either Phobos or Deimos. The zero eccentricity families of periodic orbits have been constructed and found to be stable. The most important resonant orbits in the nonzero eccentricity case have also been found. Injection sensitivity studies show broad error limits in injection position, but injection velocity must be tightly controlled. Stable retrograde orbits exist about both moons, staying in the moons' vicinity for at least 25 days, and quite probably longer. Some thoughts on a Mars' moon orbiter mission have been offered.

References

[1]Dobrovolskis, A. R., and Burns, J. A., "Life Near the Roche Limit," *Icarus*, Vol. 42, 1980, pp. 422–441.

[2]Jannson, S. W., and Wiesel, W. E., "Orbiting a Rock: Stable Orbits about Phobos and Deimos," *Proceedings of the AIAA/AAS Astrodynamics Conference* (Portland, OR), AIAA, Washington, DC, 1990, pp. 51–55 (AIAA Paper 90-2887).

[3]Luria, F., "Analysis of Periodic Orbits About the Martian Moons by Continuation Techniques," Master's Thesis, Air Force Inst. of Technology, Wright Patterson Air Force Base, OH, 1990.

[4]Meirovitch, L., *Methods of Analytical Dynamics*, McGraw-Hill, New York, 1970, p. 436.

[5]Christensen, E. J., and Balmino, G., "Development and Analysis of a Twelfth Degree and Order Gravitational Model for Mars," *Journal of Geophysical Research,* Vol. 84, 1979, pp. 7943–7953.

[6]Tolson, R. H. et al., "Preliminary Results of the First Viking Close Encounter with Phobos," *Science*, Vol. 282, 1978, pp. 697–698.

[7]Avanesov, G. A. et al., "Television Observations of Phobos," *Nature,* Vol. 341, 19 Oct. 1989, pp. 585–587.

[8]Thomas, P. C., "The Shape of Small Satellites," *Icarus*, Vol. 77, 1989, pp. 248–274.

[9]Duxbury, T. C., "The Figure of Phobos," *Icarus*, Vol. 78, 1989, pp. 169–180.

[10]Calico, R. A., and Wiesel, W. E., "Control of Time-Periodic Systems," *Journal of Guidance, Control, and Dynamics*, Vol. 7, No. 6, 1984, pp. 671–676.